ADVANCED FUNCTIONAL MATERIALS
www.afm-journal.de

Ternary Superhydrides Under Pressure of Anderson's Theorem: Near-Record Superconductivity in (La, Sc)H_{12}

Dmitrii Vladimirovich Semenok, Ivan Alexandrovich Troyan, Di Zhou,* Andrei Vladimirovich Sadakov, Kirill Sergeevich Pervakov, Oleg Alexandrovich Sobolevskiy, Anna Gennadievna Ivanova, Michele Galasso, Frederico Gil Alabarse, Wuhao Chen, Chuanying Xi, Toni Helm, Sven Luther, Vladimir Moiseevich Pudalov, and Viktor Viktorovich Struzhkin**

Lanthanum-hydrogen system and its derivatives hold significant promise for achieving room-temperature superconductivity. In this study, the formation of ternary lanthanum-scandium superhydrides is examined at pressures up to 220 GPa. The primary product of the LaSc alloy's reaction with hydrogen is a newly discovered cubic (La,Sc)H_{12}, demonstrating a clear superconducting transition in all six channels of the van der Pauw-contact scheme at 244–248 K. In this compound with an unusually large unit-cell volume, virtually no magnetoresistance is observed in fields up to 68 Tesla. Synthesized samples of (La,Sc)H_{12} demonstrate pronounced superconducting diode and SQUID-like effects at a record high temperature of 233 K, which opens up prospects for the use of superhydrides in compact electronics. Furthermore, the analysis reveals the possible formation of a lower hexagonal polyhydride (La,Sc)$H_{6\text{-}7}$, which can potentially account for the drop in electrical resistance observed near 274 K. This anomaly between 265–290 K also appears in the radio-frequency transmission measurements and may be of a superconducting nature.

1. Introduction

Pressure-stabilized polyhydrides are a new rapidly growing class of high-temperature superconductors.[1,2] Remarkable properties of H_3S (critical temperature, T_c = 200 K),[3] YH_6 (T_c = 224 K)[4] and LaH_{10} (T_c = 250 K)[5,6] at 130–200 GPa catalyzed the search for superconductivity (SC) in compressed ternary (X,Y)-H polyhydrides that can be obtained by pulsed laser heating of various alloys and intermetallics with hydrogen or ammonia borane (AB, NH_3BH_3) in diamond anvil cells (DACs). The uniquely high critical temperatures, upper critical magnetic fields up to 300 T[7] and critical current densities of superhydrides are very attractive for the creation of new electronic

D. V. Semenok, D. Zhou
Center for High Pressure Science & Technology Advanced Research
Bldg. #8E, ZPark, 10 Xibeiwang East Rd, Haidian, Beijing 100193, China
E-mail: dmitrii.semenok@hpstar.ac.cn; di.zhou@hpstar.ac.cn

V. V. Struzhkin
Shanghai Key Laboratory of Material Frontiers Research in Extreme Environments (MFree)
Shanghai Advanced Research in Physical Sciences (SHARPS)
68 Huatuo Rd, Bldg #3, Pudong, Shanghai 201203, China
E-mail: viktor.struzhkin@hpstar.ac.cn

V. V. Struzhkin
Center for High Pressure Science & Technology Advanced Research
1690 Cailun Rd, Bldg #6, Pudong, Shanghai 201203, China

I. A. Troyan, A. G. Ivanova
A.V. Shubnikov Institute of Crystallography of the Kurchatov Complex of Crystallography and Photonics
59 Leninsky Prospekt, Moscow 119333, Russia

A. V. Sadakov, K. S. Pervakov, O. A. Sobolevskiy, V. M. Pudalov
V. L. Ginzburg Center for High-Temperature Superconductivity and Quantum Materials
53 Leninsky Prospekt, building 10, Moscow 119991, Russia

M. Galasso
Institute of Solid State Physics
University of Latvia
8 Kengaraga str., Riga LV-1063, Latvia

F. G. Alabarse
Elettra Sincrotrone Trieste
Strada Statale 14 km163,5 in AREA Science Park, Basovizza, Trieste 34149, Italy

W. Chen
Quantum Science Center of Guangdong–Hong Kong–Macao Greater Bay Area (Guangdong)
Shenzhen 518045, China

C. Xi
Anhui Province Key Laboratory of Condensed Matter Physics at Extreme Conditions
High Magnetic Field Laboratory of the Chinese Academy of Science
Hefei, Anhui 230031, China

T. Helm, S. Luther
Hochfeld-Magnetlabor Dresden (HLD-EMFL) and Würzburg-Dresden Cluster of Excellence
Helmholtz-Zentrum Dresden-Rossendorf (HZDR)
Bautzner Landstraße 400, 01328 Dresden, Germany

The ORCID identification number(s) for the author(s) of this article can be found under https://doi.org/10.1002/adfm.202504748

DOI: 10.1002/adfm.202504748

devices based on high-pressure DACs. The general and as yet unsolved problem of ternary superhydrides boils down to the question: "Can T_c in ternary polyhydrides be higher than in binary ones and reach room-temperature values?". As the analysis of the thermodynamic stability of the SC state shows, from a fundamental point of view there is no reason why room-temperature superconductivity cannot be achieved in compressed polyhydrides.[8–10]

Anderson's theorem[11,12] exerts considerable pressure on the experimental search for new high-temperature superconductors in (pseudo)ternary and high-entropy[7] hydride systems, which are perhaps its best illustration.[13] The problem is that the synthesis of hydrides via the laser heating inevitably leads to random mixing of heavy atoms in their sublattice with the formation of solid solutions.[14] A rather long list of already experimentally investigated ternary systems can be given, where the introduction of a third element just slightly changes the critical temperature: (La,Y)H_{10},[14] (La,Y)H_4,[15] (La,Ca)H_{10},[16] (Y,S)H_9 and (Y,S)H_6,[17] (La,Al)H_{10},[18] (La,Be)H_8.[19]Moreover, in the case of introduction of atoms with *f*-electrons a significant decrease of T_c is observed: (La,Nd)H_{10},[13] (Y,Ce)H_x,[20] and (La,Ce)$H_{9\text{-}10}$[21,22] serve as examples. The recent synthesis of the ordered (truly) ternary hydride LaB_2H_8[23] also does not solve the problem, since its T_c is only slightly higher than that of LaH_4[21] or La_4H_{23}.[24,25] A solution to this problem may be a "cold" synthesis route from pure H_2 and intermetallics, in which the heavy atoms remain in their positions and the hydrogen slowly diffuses and dissociates in the metallic sublattice.

In this work, we turn our attention to the La-Sc-H system at pressures up to 230 GPa. In this system, the room-temperature superconductivity has recently been predicted for both the binary phase $Pm\bar{3}$-ScH_{12}[26] and for the ternary one *P*6/*mmm*-$LaSc_2H_{24}$[27] (XH_8 type). Partial substitution of La atoms by Sc in LaH_{10} was discussed by Kostrzewa et al. [28] indicates a significant increase in T_c up to 294 K. The experiment indeed shows the formation of a (La,Sc)H_{12} with T_c = 244–248 K, however, with a different symmetry of the cubic lattice (*fcc*). Samples of (La,Sc)H_{12} exhibit a pronounced diode effect and SQUID-like resistance oscillations[29] accompanied by the disappearance of residual resistance below 215 K in all six van der Pauw channels. Moreover, we found a partial drop in electrical resistance at 274 K in one of the (La,Sc)H_x samples, and anomalies, typical for superconductivity, in the radio-frequency transmission of lanthanum-scandium hydrides in the range of 265–290 K.

2. Results and Discussion

We studied six samples of La-Sc hydrides under pressure: DACs LS-1, LS-2 were prepared for the room- and low-temperature X-ray diffraction (XRD) measurements, DACs LS-3, LS-5 were designed for pulsed magnetic fields, DAC LS-4 was intended to study the dependence of critical temperature on pressure. Finally, DAC LS-6 contained two Lenz lenses and was prepared for radio-frequency transmission measurements. In all cases except LS-5, a La-Sc 1:1 alloy, obtained by sintering of La and Sc metal powders in an argon arc, was used. To load the DAC LS-5, we used La:Sc 1:2 alloy, prepared by the same method. The composition and homogeneous distribution of elements in the LaSc alloy were confirmed by X-ray fluorescent (XRF) and energy dispersive X-ray (EDX) analysis (Figure 2B; Figures S3–S5, Supporting Information). Ammonia borane (AB, NH_3BH_3) was used as a source of hydrogen. Laser heating of samples was carried out through a series of ≈0.3 s infrared laser pulses (λ = 1.06 μm), in which the sample temperature increased to at least 1000–1500 K leading to the decomposition of AB. In general, the DACs preparation and transport measurements are similar to our previous works.[30] A detailed description of high-pressure DACs is given in Supporting Table S1 (Supporting Information).

2.1. Synthesis of La-Sc Polyhydrides at 189–196 GPa

Powder X-ray diffraction (XRD) combined with first-principles calculations of the unit cell volume, thermodynamically stable structures, and electron-phonon mediated superconductivity is the standard method for establishing the structure of superhydrides.[1,31] This led to the choice of XRD as the first step of our research.

X-ray diffraction study of a DAC LS-1 sample synthesized at 196 GPa shows the presence of a cubic ($Fm\bar{3}m$) phase as the main reaction product (**Figure 1A**). But what is surprising is the unit cell volume of the resulting compound: almost 32 Å^3 per metal atom exceeds the expected volume of the LaH_{10} at 196 GPa. Given that 50 ± 5% of the alloy consists of much smaller Sc atoms, we have to attribute a larger amount of hydrogen to the chemical formula of this compound. It should be given by (La,Sc)$H_{12\pm x}$, where x is about 1. For simplicity, we will further use the chemical formula (La,Sc)H_{12} for this compound. Indeed, *fcc*-ScH_3 at 140 GPa has a unit cell volume 15.05 Å^3/Sc,[32] whereas *fcc*-LaH_3 at the same pressure has the volume of 20.5 Å^3/La.[5] Therefore, the difference in the volumes V(La) –V(Sc) is 5.45 Å^3 per atom at 140 GPa. If we take this difference into account and consider a slight decrease in cell volumes during compression to 2 Mbar, the amount of hydrogen in the resulting compound will be equivalent to the same in LaH_{12}.[5,33] This also corresponds to the unusually large unit cell volume of "$LaH_{10+\delta}$" obtained from single-crystal X-ray analysis of lanthanum polyhydrides.[34] Moreover, we believe that La superhydride with the canonical formula "LaH_{10}" is rare in experiments. Instead, since the earliest works, it demonstrates variability in composition within the range of $XH_{9\text{-}12}$,[35] at the same time maintaining a maximum critical temperature of at least 240–250 K. This amazing constancy of the maximum T_c, which does not depend neither on randomly distributed impurities (B, N, Al, Ca, Y, Sc ...), nor on the method of obtaining La superhydride, nor on variations in the composition of hydrogen (±1–2 H atoms), is, in our opinion, one of the most striking manifestations of Anderson's theorem for the Bardeen–Cooper–Schrieffer (BCS) superconductors.[11]

Due to the absence of additional X-ray reflections from the scandium sublattice, we will further consider the (La,Sc) solid solution model for the heavy atom sublattice. This situation is common for many ternary polyhydrides.[13,14,16,21,22] There is no doubt that several other phases are present in the sample, as the number of peaks exceeds that for both the $Fm\bar{3}m$-(La,Sc)H_{12}, as well as the number of reflections for a distorted phase *F(P)mmm*-(La,Sc)H_{12} (see Figures S7 and S8, Supporting Information). The latter one is likely formed due to the large difference in volumes and properties of La and Sc atoms. The existence of side phases

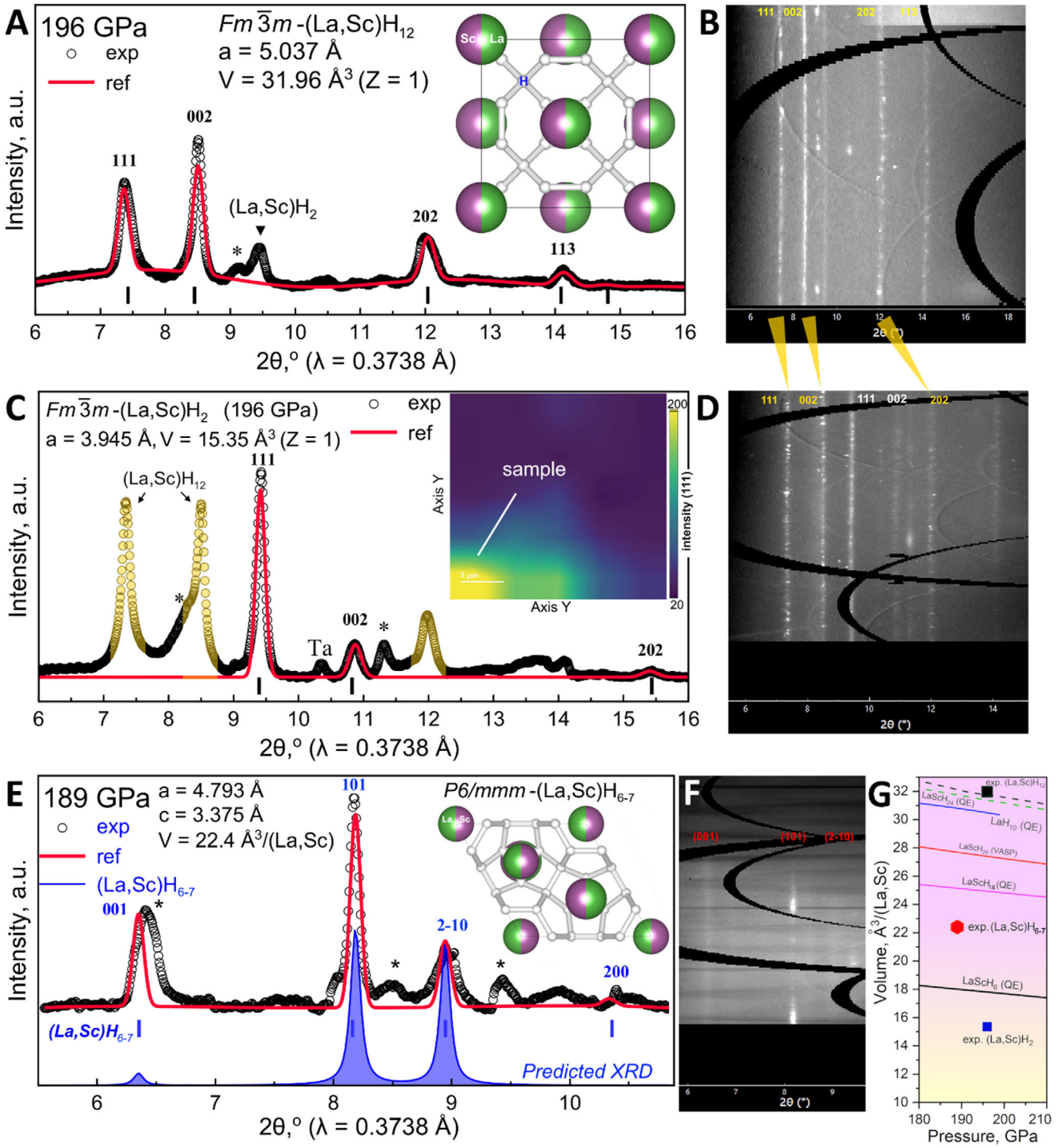

Figure 1. Powder X-ray diffraction analysis and the Le Bail refinements of the unit cell of (La,Sc)H_{12}, (La,Sc)H_7 and (La,Sc)H_2 phases in DACs LS-1 and LS-3 at 189–196 GPa. A) Le Bail refinement of the unit cell parameters of *Fm*$\bar{3}$*m*-(La,Sc)H_{12} (JANA2006) in DAC LS-1: black points mark experimental data, the red line – is the refinement. Inset: structural model of this compound based on a cubic La sublattice of LaH_{10}. Asterisks mark unexplained reflections. B) X-ray diffraction image ("cake") of the sample in DAC LS-1. C) Experimental XRD and Le Bail refinement of the unit cell parameters of *Fm*$\bar{3}$*m*-(La,Sc)H_2 synthesized in the DAC LS-1 (JANA2006). Yellow color marks reflections from *the Fm*$\bar{3}$*m*-(La,Sc)H_{12}. "Ta" indicates a possible peak from Ta/Au electrodes. The inset shows the spatial distribution of the (La,Sc)H_{12} 111 reflection. D) Typical X-ray diffraction image ("cake") which contains reflections from both (La,Sc)H_2 and (La, Sc)H_{12}, DAC LS-1. E) Experimental XRD pattern and Le Bail refinement of the unit cell parameters of (La,Sc)H_{6-7} found in DAC LS-3. Filled blue plot – is calculated XRD pattern for predicted *P6/mmm*-$LaSc_2H_{24}$ with solid solution of (La, Sc) in metal sublattice. F) X-ray diffraction image ("cake") of the sample in DAC LS-3. G) Calculated equations of state (QE, VASP codes) and experimental unit cell volumes used to estimate the H-content in obtained compounds.

in the sample also follows from the presence of several steps in the observed SC transitions (Figures 3, 4). Additional XRD reflections may appear from Ta/Au electrodes and from the lower hydride $Fm\bar{3}m$-(La,Sc)H_2 (Figure 1C).

The X-ray diffraction study of the sample in the DAC LS-3 at 189 GPa was limited by the small diameter (d = 15.3 mm) of this highly asymmetric cell intended for studies in pulsed magnetic fields. The result of the XRD measurements was unexpected: instead of the usual $Fm\bar{3}$ m-like pattern we discovered a hexagonal pattern that can be refined as $P6/mmm$ (Figure 1E). Recently, a similar structure, $P6/mmm$-$LaSc_2H_{24}$ (XH_8 type), was predicted to be a room-temperature superconductor with T_c = 316 K below 200 GPa.[27] This compound has a calculated unit cell volume of 24.15 Å^3/(La, Sc) at 200 GPa[27] which is significantly less than the expected volume of LaH_8 due to the smaller volume of the Sc atom. The experimental cell volume of the phase (La,Sc)H_x that we obtained in DAC LS-3 is 22.4 Å^3/(La, Sc) at 189 GPa despite the higher content of La. This indicates that the hydrogen content is less than in the predicted $LaSc_2H_{24}$ and its chemical formula is close to (La,Sc)H_{6-7}. As we will see below, presence of this hexagonal phase in DAC LS-3 may be reflected in the temperature dependence of the electrical resistance, demonstrating a pronounced drop at ≈ 274 K, noticeably higher than T_c of cubic (La,Sc)H_{12} phase (Figures 3 and 4a). However, it should be noted that an additional experiment with $LaSc_2$ alloy, conducted in DAC LS-5 at 188 GPa, showed only traces of a series of superconducting transitions (Supporting Figure S28, Supporting Information).

2.2. Synthesis of La-Sc Polyhydrides at 150–153 GPa. Low-Temperature XRD

In 2020–2021, it was suggested that compressed hydrides may not be superconductors, and resistive transitions in them are a consequence of structural phase transitions.[36] This suggestion was facilitated by the absence of X-ray diffraction data near observed transition temperatures. The lack of structural information motivated our low-temperature X-ray diffraction experiment with (La,Sc) hydrides at 153–169 GPa performed at the Xpress beamline of the Elettra synchrotron radiation facility. Gold piece was used as the pressure gauge in these experiments.

In this part of the work, we synthesized La-Sc ternary hydrides at 150–153 GPa (**Figure** 2A) in DAC LS-2 from the corresponding 1:1 La-Sc alloy, the XRF and EDX analysis of which is shown in Figure 2B, Figures S3–S5 (Supporting Information). The main product of the reaction at this pressure can be refined using hexagonal structures, for example, via $P6_3/mmc$-ScH_6, predicted by Hou et al.[37] However, the ratio c/a = 1.26 is unusual for this space group (Figure 2C). The unit cell volume of obtained compound is 21.85 Å^3/(La, Sc) which indicates composition of (La, Sc)H_{6-x} similar to the predicted hexagonal ScH_6.[37] We believe that the proposed $P6_3/mmc$ structure describes well the resulting diffraction pattern except for an unexpectedly low intensity of the (101) reflection (Figure 2B), and can serve as a first approximation for further structural analysis. Comparison of the experimental unit cell volume, 21.85 Å^3/(La, Sc), with the theoretical calculation (V_{DFT} = 23.64 Å^3/(La, Sc)) shows that the hydrogen content in this hexagonal phase is between 5 and 6 per metal atom. It should be noted, that the intensity of the XRD pattern in low-temperature cryostat appears insufficient to accurately refine the unit cell parameters at all studied pressure points (Table S3, Supporting Information).

The DAC LS-2 was cooled to a temperature of 150 K while low-temperature powder XRD was recorded. No obvious phase transitions were observed between 150–300 K and 153–169 GPa (Figure 2E). However, there are some signs of small distortion of the crystal lattice at 200–250 K: splitting of the 100 reflection and anomaly of the c/a ratio (Figure 2E, Table S3, Supporting Information). When cooled to 100 K, the pressure in DAC LS-2 increased above 170 GPa that caused collapse of diamond anvils followed by the pressure drop to 30 GPa. The XRD pattern obtained at 30 GPa and 300 K indicates a significant change in the structure and H-content of the (La,Sc) hydrides, and can be described as a two-phase mixture consisting of tetragonal $I4/mmm$-(La,Sc)H_{3-x} (phase I) and thermodynamically stable, pseudocubic $P4_1$-(La,Sc)$H_{\sim 3}$ (phase II, Tables S3 and S7, Supporting Information). The deviation from the calculated unit cell volumes of (La,Sc)H_{3-x} and (La,Sc)H_3 indicates the non-stoichiometric composition of the obtained compounds. We should note again that the X-ray beam intensity is not sufficient for a qualitative interpretation of the diffraction data. The main conclusion from this low-temperature XRD experiment is that high-T_c superconductivity in the La-Sc-H system is not accompanied by pronounced phase transitions at temperature above 150 K.

Therefore, the X-ray diffraction study of the La-Sc-H system indicates possible presence of polyhydrides which are similar to the predicted ones: these are hexagonal $LaSc_2H_{24}$,[27] ScH_6,[37] and cubic ScH_{12}.[26] Indeed, in the experiment we see the cubic phase (La,Sc)H_{12}, the hexagonal phases (La,Sc)H_{6-7} and (La,Sc)H_{6-x} at 150 GPa. It was already noticed (for instance, in Refs. [30,38]) that structural search programs such as USPEX,[39–41] CALYPSO,[42,43] AIRSS[44,45] are good at calculating the hydrogen content of stable polyhydrides, whereas the prediction of correct crystal symmetry is much more difficult. And in our experiments we encountered exactly this situation: we see La-Sc hydrides with the predicted stoichiometry, but with an unexpected lattice symmetry. Despite this drawback, first-principles methods provide important clues to the interpretation of products of high-pressure synthesis.

2.3. Superconductivity of La-Sc Polyhydrides

Transport properties of La-Sc hydrides at 196 GPa were studied in high-pressure DACs LS-1 and LS-3. We used diamond anvils with a culet diameter of 50 µm, equipped with four sputtered (Ta/Au) electrodes and tungsten gasket covered by CaF_2/epoxy insulating layer. For a detailed description of the experiment, see Supporting Information. The studies were performed in both direct current (DC, **Figure** 3A), and alternating current (AC) modes. Regardless of the test method chosen, (La,Sc)H_{12} sample in DAC LS-1 shows a disappearance of electrical resistance below 235 K (Figure 3A). Transport measurements (Figure 3A,D) indicate the possible presence of two phases in the sample, with close critical temperatures: T_c(onset) ≈ 247–248 and 242 K (see also Figure 5F). The broadening of superconducting transitions in magnetic fields up to 16 T is insignificant, as for many other polyhydrides[46] which is associated with a high concentration of

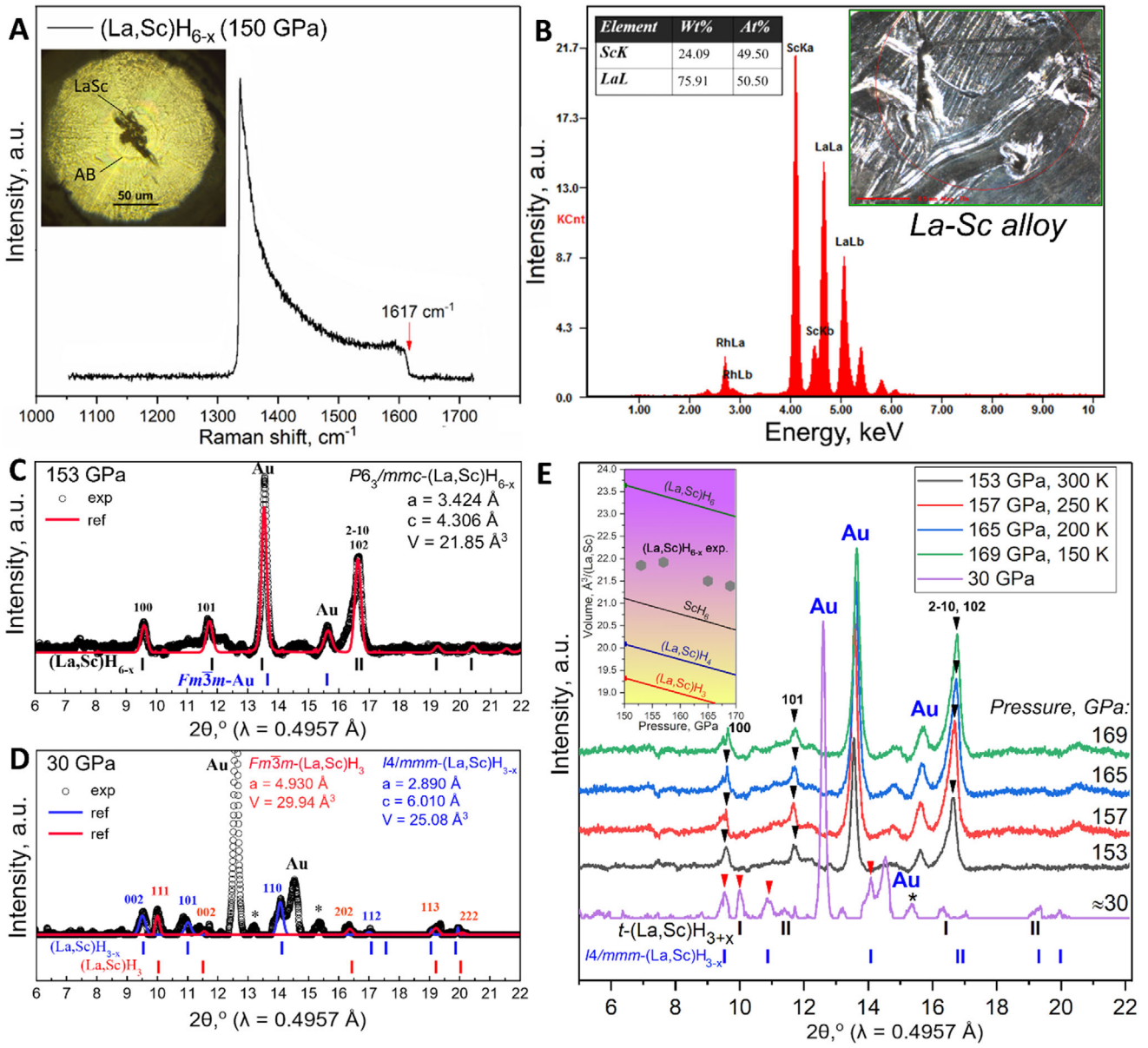

Figure 2. Synthesis and X-ray diffraction of La-Sc hydrides in DAC LS-2 at 150–153 GPa. A) Raman spectrum of the sample in DAC LS-2 in the region of C-C vibrations after laser heating. Inset: photo of the sample. B) X-ray fluorescence analysis of initial La-Sc alloy. Composition is close to 1:1 (see Table in the inset). C) Experimental X-ray diffraction patterns and Le Bail refinements of unit cell parameters of hexagonal (La,Sc)H_{6-x} at 153 GPa (300 K). "Au" – denotes reflections from gold used as the internal pressure sensor. Asterisks indicate uninterpreted peaks. D) The same for tetragonal (La, Sc)H_{3-x} and pseudocubic (La, Sc)H_3 at 30 GPa after collapse of the DAC LS-2. E) A series of XRD patterns of the DAC LS-2 sample taken during decreasing temperature from 300 to 150 K with a step of 50 K. As it cooled, the pressure in the DAC spontaneously increases with $dP/dT \approx -0.11$ GPa/K. The pattern at 30 GPa corresponds to a broken DAC.

defects, pinning centers and very high depinning potential barriers reaching in hydrides 1–2 × 10^5 K.[47,48] This correlates with virtually zero magnetoresistance (MR) over the studied range of temperatures (170–223 K) and magnetic fields (Figure 3E).

In some cases, non-uniform distribution of sample conductivity in the van der Pauw circuit leads to "false" voltage (resistance) drops, which actually correspond to a local increase in the resistivity.[36] Such voltage drops may be incorrectly interpreted as superconducting transitions. In this situation, it is necessary to examine all combinations of electrodes. For a four-electrode circuit there are six different channels, two of them are "diagonal" (or the Hall type). Results of measuring the voltage drop across the (La, Sc)H_{12} sample at 196 GPa on four off-diagonal electrode combinations vdp1-4 are presented in Figure 3A,B. In the region of the SC transition, the resistance decreases from ≈ 0.1 Ω to 1–2 μΩ, that is, by a factor of 10^5. The thermal noise of the measuring circuit is symmetrical on all four channels. Moreover, the diagonal channels (*diag1,3* and *diag2,4*, see Figure S11, Supporting

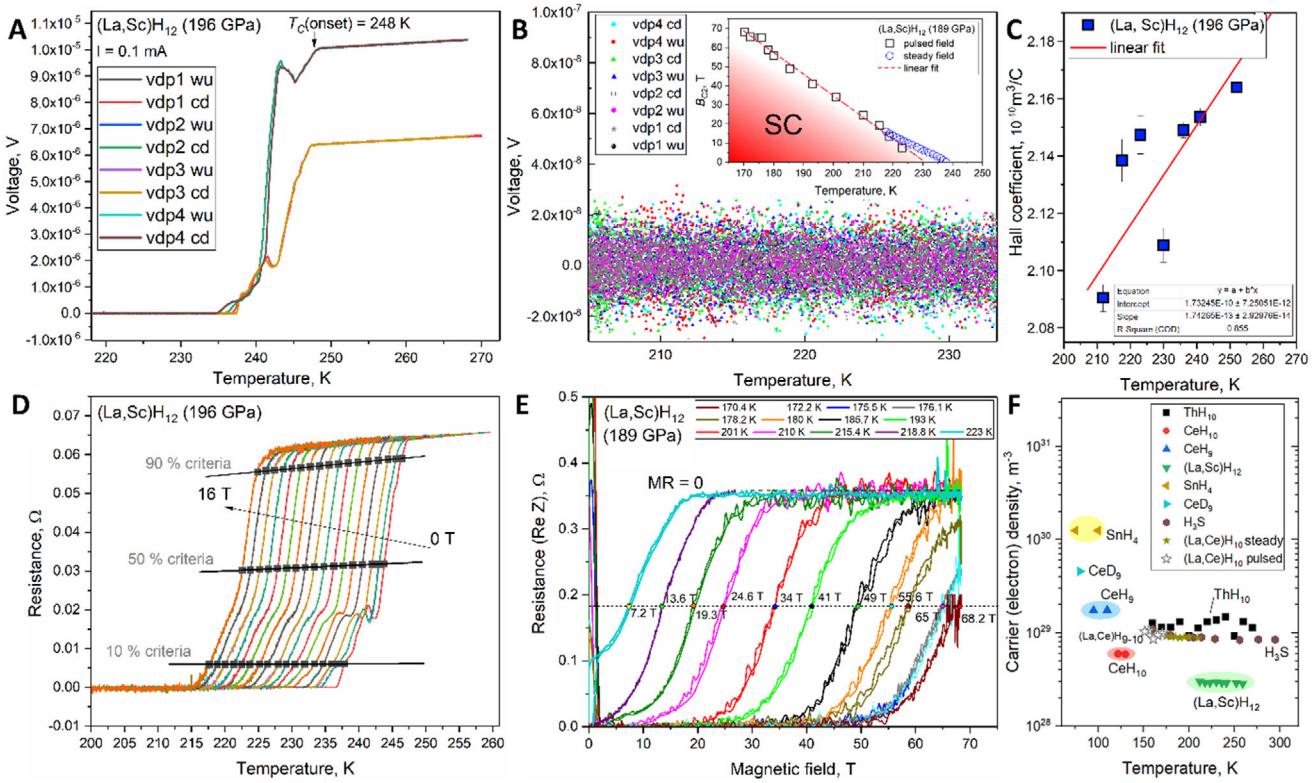

Figure 3. Transport properties of (La, Sc) hydrides at 189 and 196 GPa in steady and pulsed magnetic fields. A) Dependence of the voltage drop across the DAC LS-1 sample (La, Sc)H_{12} on temperature in the warming ("wu") and cooling ("cd") cycles for four direct channels of the van der Pauw circuit (vdp1-4). Here we used the delta mode with a DC excitation current of 0.1 mA. B) Residual voltage on the sample after transition to the superconducting state on four direct channels (vdp1-4) in the cooling and warming cycles. Average residual resistance of the sample is ≈ 1-2 μΩ. Inset: the boundary of the SC and non-SC regions on the phase diagram, as well as the $B_{C2}(T)$ temperature dependence in magnetic fields up to 68 T, the $R_{50\%}$ criterion was applied. C) Temperature dependence of the absolute value of Hall coefficient in (La, Sc)H_{12} at 196 GPa ("C" stands for Coulomb, the unit of charge). Steady fields ± 33 T were used for measurements. Red line – is the linear fit. D) Temperature dependence of the electrical resistance of the (La, Sc)H_{12} in various constant magnetic fields from 0 to 16 Tesla. The criteria $R_{10\%}$, $R_{50\%}$, $R_{90\%}$ were applied to determine $B_{C2}(T)$. E) Dependence of the real component of the electrical resistance of the sample in DAC LS-3 on a pulsed magnetic field up to 68 T at various temperatures from 223 K to 170.4 K. "MR" denotes magnetoresistance. F) Carrier (electron) concentration in various superhydrides according to the Hall coefficient measurements: $n_e = 1/eR_H$. Thickness of initial LaSc foil is assumed 1 ± 0.5 μm based on the visible light interference pattern between diamond anvils before compression.

Information) also show the disappearance of the sample's electrical resistance and symmetrical residual thermal noise. The obtained result excludes the possibility of any metal-insulator transitions in the sample.

We studied the behavior of La-Sc hydrides in steady (0 – 33 T, DAC LS-1) and pulsed magnetic fields with a pulse duration of 150 ms and maximum field induction of 68 T (DAC LS-3). Since the primary superconducting transition in DAC LS-3 sample is observed at the $T_c \approx 244$ K (**Figure** 4A), we will henceforth consider (La,Sc)H_{12} to be the main content of the LS-3 sample despite the fact that we were unable to detect this phase using XRD analysis due to the limited opening angle in this asymmetric DAC. Such a strong pulsed magnetic field was used to establish the shape of the superconducting phase diagram (inset in Figure 3B). In this case, measurements of the dependence of the electrical resistance (real part, Re Z) on the magnetic field were carried out in AC mode at frequencies of 16.66 kHz and 33.33 kHz in the temperature range from 170.4 K to 223 K (inset in Figure 3E). In this range of temperatures and fields, the magnetic phase diagram of (La,Sc)H_{12} is linear ($dB_{C2}/dT \approx -1.15$ T/K), as for many other hydrides.[13,49,50,51] Very high upper critical field $B_{C2}(0)$ of La-Sc superhydrides is remarkable. The extrapolated value of $B_{C2}(0)$ can exceed 200–230 T (Figure 3B). Such a high upper critical field is characteristic of dirty ("hard") superconductors and high-entropy polyhydrides.[7]

Metal superhydrides synthesized at high pressure are, in most cases, fine powders[52] with a large number of defects in microcrystals.[1,13,30,52] This determines many physical properties of hydrides. For example, wide diffusive XRD patterns,[38,53,54] very low RRR (residual-resistance ratio) about 1.1–1.5,[4] and often near zero magnetoresistance. Typically, the magnetoresistance of metals is positive and $\propto \mu_e^2 B^2$, where μ_e is the electron mobility (in the absence of holes). However, hydrides are different. The existence of a region of negative magnetoresistance was established in La_4H_{23}[24,25] and CeH_{10},[55] whereas magnetoresistance of (La,Sc)H_{12} in DAC LS-3 is practically equal to zero like in graphene.[56]

One of the most likely explanations of this fact is a very defective and finely dispersed structure of the sample containing B, and N impurities from ammonia borane, fluctuations of Sc and

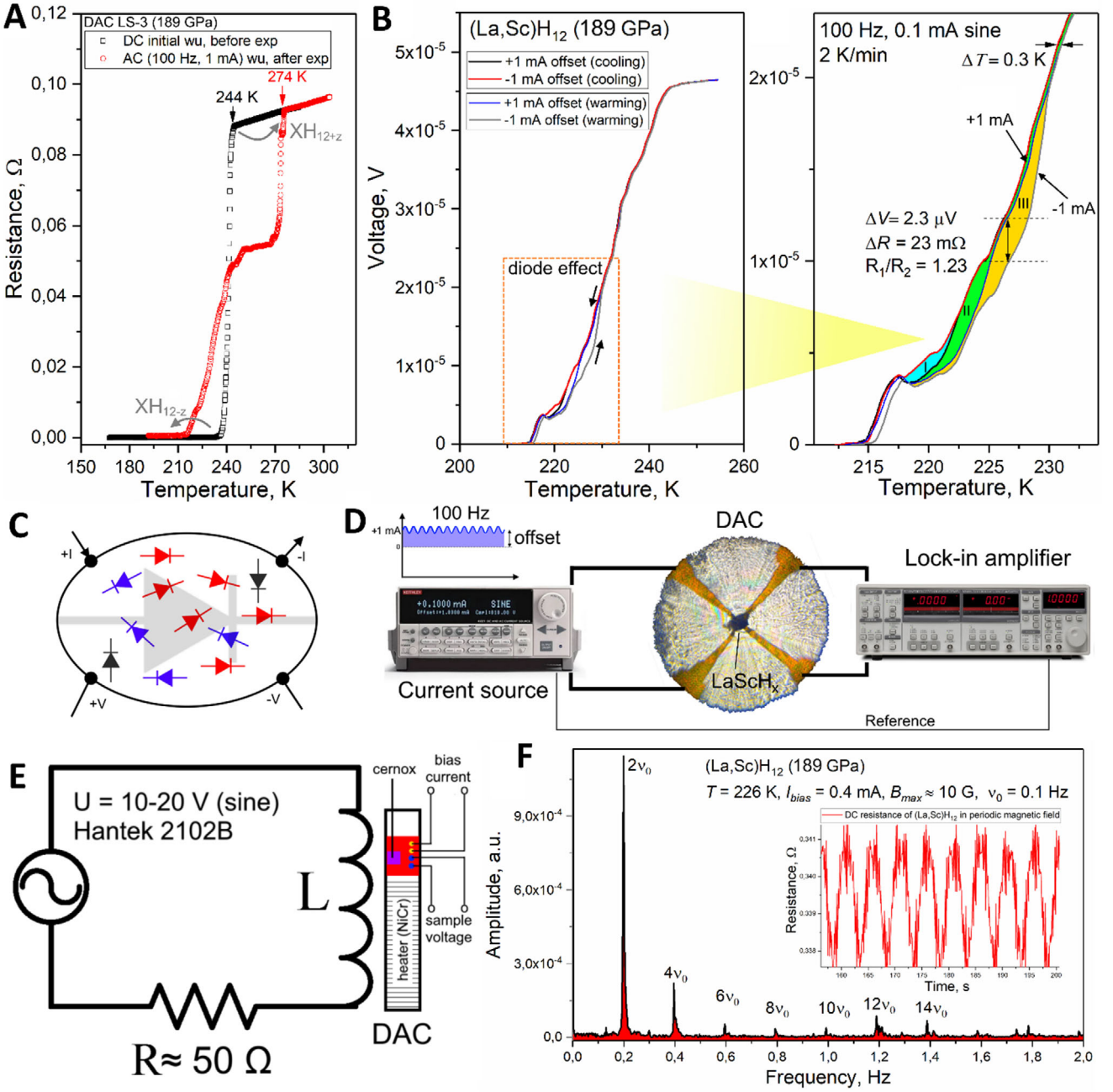

Figure 4. Diode and DC SQUID effects in (La,Sc)H_{12} (DAC LS-3). A) Stable (black circles) and "metastable" (red circles) resistive transitions in the La-Sc superhydride at 189 GPa. The arrow indicate a possible electrochemical process of hydrogen migration between electrodes, leading to broadening of the SC transition and the appearance of new metastable phase. The resistance ratio R_1/R_2 allows us to estimate the ratio of the lengths of the current paths in low-T_c and high-T_c phases as 60:40. B) Diode effect observed in the sample when applying an offset DC current of +/– 1 mA. Area I (azure) corresponds to the hysteresis of the sample resistance when the offset current changes its sign in a cooling cycle (2 K min^{-1}). Area II (green) corresponds to the resistance hysteresis at a constant offset +1 mA, occurring between heating and cooling cycles. Area III (yellow) corresponds to the hysteresis of the sample resistance when the current offset sign changes in the warming cycle (2 K min^{-1}). C) Schematic illustration of the random arrangement of asymmetric conductivity regions in the sample. D) Experimental scheme of measurements of the diode effect, which excludes the contribution of thermo EMF. E) Scheme of studying the SQUID effect in the sample when a weak modulated magnetic field (≈ 10 G) is applied. F) Generation of higher harmonics when the (La,Sc)H12 SQUID resistance changes in response to a periodic weak external magnetic field. Inset: complex periodic pattern of the electrical resistance versus time.

La concentration like in NbTi,[57] presence of H_2 molecules and H vacancies. In this case, the electron mean free path (l_e) is significantly less than the Larmor radius (r_g) even at 70 T

$$l_e \ll r_g = \frac{m_e^* v_F}{eB} \quad (1)$$

where the Fermi velocity v_F can be estimated as $\approx 3 \times 10^5$ m $^{-1}$s,[58] and m_e^* is the effective electron mass. If we take $m_e^* = m_e$ and magnetic field induction $B = 50$ T, then $r_g \approx 38$ nm. This value should be comparable to the crystallite size and the average distance between defects in (La, Sc)H_{12}. In this case, scattering on defects and grain boundaries will be the dominant process, and the influence of the magnetic field will be insignificant. Of course, it cannot be completely ruled out that the positive magnetoresistance ($\propto \mu_e^2 B^2$), observed due to the distortion of electron trajectories in a magnetic field, can compensate for negative magnetoresistance related to the preformation of Cooper pairs, giving an ultimately zero result in a certain range of magnetic fields.

Finally, we have studied the Hall effect and its sign in the non-superconducting state of (La, Sc)H_{12} in DAC LS-1. In the Hall measurement scheme, the superconducting transition begins at the same T_c around 245 K, but is accompanied by a more complex behavior of the electrical resistance *R(T, B)*. Figures S12–S14 (Supporting Information) show that the Hall voltage depends on a magnetic field linearly. The Hall coefficient R_H is found negative. This indicates that electrons are the primary charge carriers. $|R_H| = (2.13 \pm 0.03) \times 10^{-10}$ m^3 C^{-1} in (La, Sc)H_{12} slightly decreases along with temperature (Figure 3C). This corresponds to an increase of carrier concentration by 3% during cooling from 259 to 212 K: n_e((La,Sc)H_{12}) = $1/eR_H = (2.95 \pm 0.05) \times 10^{28}$ m^{-3} (Figure 3F). In general, almost temperature independent carrier concentration is typical for metals. The found values of electron concentration n_e((La,Sc)H_{12}), within the accuracy of the error in determining the sample thickness, are similar to the concentration of carriers in other superhydrides (Figure 3F). Alternatively, the increase in the Hall resistance with temperature may be due to the interaction quantum corrections (Altshuler-Spivak corrections), which in the diffusion regime for a high concentration of electrons and, especially, in strong magnetic fields, must have a positive sign $dR_H/dT > 0$, the same as that of the diagonal component of the resistance.

2.4. Metastable Resistive Transitions, SQUID-Like, and Diode Effects in (La, Sc)H_{12}

When studying the Hall effect in the DAC LS-3, we found unexpectedly that the onset of the resistance drop at a certain stage of the experiment shifted to higher temperatures, reaching unusually high value of 274 K (Figure 4A; Figure S24, Supporting Information). At the same time, the main superconducting transition, probably corresponding to the (La, Sc)H_{12}, was still observed at $T_c = 244$ K. According to the Figure 4a, the ratio of partial drops of electrical resistance R_1/R_2 allows us to estimate the ratio of the current path lengths in low-T_c and high-T_c phases as ≈ 40:60. This works when both phases have a similar resistivity. However, due to the fact that the electric current passes only through a small part of the sample, it is impossible to establish the exact reaction product ratio only from the resistance data. The relatively high measurement current (1 mA, Figure 4a) that we used and the narrow transition at 274 K most likely exclude filamentary superconductivity (as, for example, in some nickelates[59]). The pronounced signal in the radio-frequency transmission (**Figure 5**) also argues against filamentary superconductivity.

High-temperature superconductivity with $T_c > 270$ K was predicted in both cubic sc-ScH_{12}[26] and hexagonal $LaSc_2H_{24}$.[27] Calculations for the last compound taking into account the anharmonic corrections lead to T_c(Allen-Dynes) = 262 K ($\mu^* = 0.1$) at 200 GPa.[60] Considering the rescaled Coulomb pseudopotential $\mu^*_{ME} = 0.16$[61] in solving the Migdal-Eliashberg[62,63] equations results in a higher $T_c = 291$ K. As can be seen from Figures 4a and 5f,g, the theoretically predicted range of 262–291 K corresponds well to the region of observed transitions in electrical resistance and radio-frequency transmission anomalies.

Despite the fact that detected resistance anomaly at 274 K correlates with the presence of a similar hexagonal phase in DAC LS-3 (Figure 1E), consideration of the recent NMR and radio-frequency transmission data on lanthanum polyhydrides[64] makes the hexagonal crystalline modifications of (La,Sc)H_{12} a more preferred explanation. Unfortunately, after 8 cooling/heating cycles (Figure S21, Supporting Information), this anomaly almost disappeared from *R-T* plots. However, some residual traces of it in the Hall measurements were found even a month after the initial detection (Figure S25, Supporting Information). As we will show in the next paragraph, this phase with the high-temperature resistive transition can be reliably detected using the radio-frequency transmission method.

Synthesized samples of La-Sc hydrides are heterogeneous. Trapping of magnetic flux by inhomogeneities in a superconducting sample[50] may lead to appearance of SQUID (superconducting quantum interference device)[29] and asymmetric conductivity effects[65] in hydrides. The later one, also known as diode effect, can be detected in (La,Sc)H_{12} superhydride (DAC LS-1) with the help of a current containing a DC offset of ± 1 mA and small sinusoidal signal of 0.1 mA (RMS) with a frequency of 100 Hz ($I(t) = \pm 1 + 0.1 \times \sqrt{2} \sin(100 \times t/2\pi)$ mA, where t – is the time). The signal amplitude at the second pair of electrodes of the 4-contact-van der Pauw circuit was detected using a lock-in amplifier SR830 and was used to calculate the sample resistance (Figure 4D,E). In this approach, all constant voltage contributions associated with thermoelectric phenomena (thermo EMF) are filtered out by the lock-in amplifier. A similar result may be obtained by a direct subtraction of the resistance data obtained for different directions of DC current (Figures S21 and S22, Supporting Information).

As a result, we found that the dependence of the electrical resistance of the sample on temperature *R(T)* has a significant hysteresis (Figure 4B,C) in the region of 220–230 K, which completely disappears above 235 K. Below this temperature there is a difference not only between curves with different directions of DC current (±1 mA), but also between the cooling and warming curves ($\Delta T > 2$ K), which indicates the presence of a "memory" effect of the sample.[66] When a direct current flows through the sample, it creates vortices in SC grains. These frozen vortices[47,48] lead to the symmetry-breaking effects and significant asymmetry ($R_+/R_- = 1.23$, at 215 K this ratio is much higher) in the sample conductivity as it observed in superconducting diodes.[65] At the same time, the effect depends on the

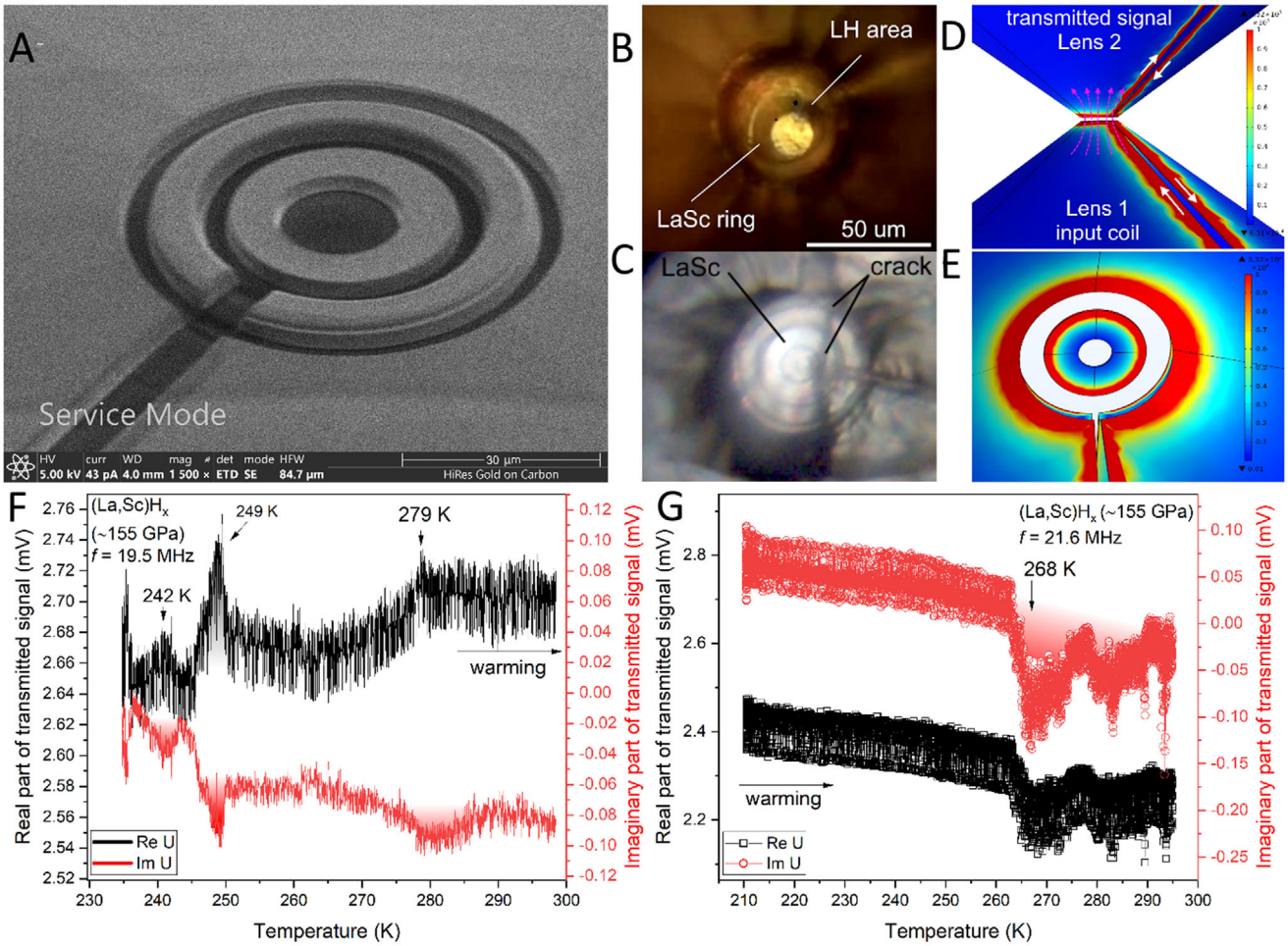

Figure 5. Radio-frequency transmittion measurements of the (La,Sc)H_x sample in the DAC LS-6. A) Scanning electron microscopy of the ring-shaped LaSc sample in the center of the Lenz lens system. B) Optical image of the sample after partial laser heating (LH), the LaSc ring is slightly displaced from the culet center. C) Photograph of the sample after partial cracking of an anvil and pressure drop to 155 GPa. D) Sketch of the RF signal transmission from Lens 1 to Lens 2 through the hydride sample. Color map corresponds to the distribution of the surface loss density (SLD) on metal surfaces. E) SLD distribution on a 60 μm ring sample at an excitation current frequency of 200 MHz. F) Real (Re U, black) and imaginary (Im U, red) parts of the transmitted signal in the warming cycle at a carrier frequency of 19.5 MHz and G) 21.6 MHz. There are pronounced features in the transmission near the known superconducting transition (240–250 K) in (La,Sc)H_{12} and in the vicinity of the previously found resistive anomaly (268–279 K).

prehistory of the sample, which stores a kind of "vortex memory" of the type of cycle (cooling or warming). The discovered diode effect is not large but is noteworthy because it opens up the possibility of creating SC diodes based on superhydrides made from LaH_{10} at record-high operating temperatures above 220–230 K.

Finally, we observed interference oscillations of electrical resistance in DAC LS-3 using a previously developed setup (Figure 4F). Application of a weak modulating magnetic field of B_{max} ≈10 G with a frequency of ν_0 = 0.1 Hz led to a generation of higher harmonics up to $14\nu_0$ already at a temperature of 226 K (Figure 4G), which is 47 K higher than the previous result achieved with (La,Ce)H_{10+x}.[29] The temperature range where the generation of higher harmonics is observed coincides with the region of the diode effect. Thus, these effects are interrelated. Moreover, measurements of the voltage drop on the DAC LS-1 sample in a magnetic field of ±300 Gauss at a temperature of 233.4 K demonstrate a pronounced periodic dependence of $R(B)$, characteristic of the DC SQUID effect in a ring with a diameter of ≈600 nm (Figure S27, Supporting Information).

The SQUID-like effect in (La,Sc)H_{12} is observed at a small bias current I_{bias} = 400–600 μA, which improves the situation with heating of the sample. This is significantly less than the 1–2 mA we had to use in the case of (La,Ce)H_{10+x}[29] and brings us closer to the currents applied in commercial SQUIDs (≈1–10 μA). Unfortunately, the size of the randomly formed SQUID-like contours was about 0.6–1 μm or less as indicated by the low sensitivity of the sample to applied magnetic field (Figures S27, Supporting Information).

2.5. Radio-Frequency Transmission Measurements

Considering the signs of a possible high-T_c superconducting transition around 274 K in the La-Sc-H system (DAC LS-3), we

performed an additional study using the radio-frequency (RF) transmission method. This highly sensitive method,[67] which we used earlier to study the La-H system in combination with high-pressure ^{1}H NMR and transport measurements,[64] allows us to detect even small-volume superconducting phases that are not in contact with the electrodes.

For this experiment, three-stage Ta/Au Lenz lenses were sputtered and cut by Ga FIB on both diamond anvils of the DAC LS-6 equipped with a 50 μm anvil culet size. These lenses allow to inductively couple the high-frequency signal to the sputtered LaSc ring (Figure 5A). During laser heating at 174 GPa, we observed a crack formation and a pressure drop in the DAC to 155 GPa (Figure 5B,C; Figure S29, Supporting Information). To prevent the further damage of anvils, the laser heating was stopped at ≈15–20% of the sample area. However, the obtained volume of superconducting phases was sufficient for further study. The experimental setup is shown in Figure S1 (Supporting Information).

The essence of the RF method in combination with the use of Lenz lenses is that the induced current flows along the surface and edges of the deposited lenses, concentrating in the area of the anvil culet with the ring sample placed on it (Figure 5D,E). At the point of the superconducting transition of the sample, a sharp change in its surface impedance is observed, which is expressed in a change in the voltage on the receiving coil and the appearance of a feature in the form of a step, peak or kink in the temperature dependence of a sample transmission. The specific shape of the feature depends on the carrier frequency (i.e., the depth of field penetration), the morphology of the sample and the distribution of superconducting phases in it, as well as on the width of the vortex liquid region in the hydride under study,[47,48] in which intense absorption of electromagnetic radiation occurs.

We investigated the temperature interval from 200 to 310 K at frequencies of 1, 10, 19.5, 21.6, and 200 MHz in the warming and cooling modes. In all the studied cases, there is a pronounced feature in the sample transmission in the range from 265 to 290 K (Figure 5F,G; Figure S29, Supporting Information), which we previously noted in the transport measurements of DAC LS-3. At some frequencies, such as 19.5 MHz, pronounced RF transmission signals are observed at 242 K and 249 K, which are characteristic of superconductivity in $Fm\bar{3}m$-(La,Sc)H_{12} (Figure 3A). It also manifests itself as a weak signal at the second harmonic ($2F = 66$ Hz) of the low-frequency ($F = 33$ Hz) modulating field in which the sample is placed. Thus, the study of the RF transmission of the (La,Sc)H_x sample in DAC LS-6 supports the conclusions of transport measurements about the presence of at least two fractions in the sample: 1) superconducting phase-I with T_c = 240–250 K, and 2) phase-II with T_c = 265–290 K. It is important to note that the obtained results are consistent with the previous reports on the possible presence of superconducting phases with the T_c of 265–280 K in the La-H system under pressure[6,68,69] (Figure S30, Supporting Information).

3. Conclusion

Our low-temperature (150–300 K, 153–169 GPa) X-ray diffraction study of superconducting lanthanum-scandium superhydrides rules out phase transitions with significant symmetry changes as a possible reason for the sharp drop of electrical resistance in the La-Sc hydrides. At 189–196 GPa we discovered a new cubic polyhydride (La,Sc)H_{12}, which demonstrates the disappearance of electrical resistance on all six channels of the van der Pauw four-contact circuit below 230 K. The onset critical temperature of this phase, which is dominant in our experiment, reaches $T_c = 248$ K. This finding is in agreement with Anderson's theorem for doped BCS-ME superconductors. In addition, La-Sc hydrides demonstrate pronounced DC SQUID-like interference oscillations of electrical resistance in a weak magnetic field, and diode effect at an unprecedented high temperature of about 233 K.

Our investigation in strong steady and pulsed magnetic fields shows that magnetoresistance of (La,Sc)H_{12} is practically absent. The extrapolated upper critical magnetic field in some heterogeneous samples may exceed 200–230 T at 0 K. The measured Hall coefficient is negative, has no features near T_c, and in absolute value ($\approx 2 \times 10^{-10}$ m^3 C^{-1}) is close to the values known for other superhydrides.

One of the (La,Sc)H_x samples at 189 GPa demonstrats an unusual "metastable" drop in electrical resistance around 274 K. This feature, together with a peak at 240–250 K, which corresponds to cubic (La,Sc)H_{12}, is also observed in the radio-frequency transmission measurements at 155 GPa in the temperature interval of 265–290 K. The potential presence of superconductivity above 0 °C in the La-Sc-H system calls for further research.

4. Ethical Statement

There are no human subjects in this article and informed consent is not applicable.

Supporting Information

Supporting Information is available from the Wiley Online Library or from the author.

Acknowledgements

D.S. and D.Z. thank National Natural Science Foundation of China (NSFC, Grant No. 12350410354) and Beijing Natural Science Foundation (Grant No. IS23017) for support of this research. D.Z. thanks China Postdoctoral Science Foundation (Certificate No. 2023M740204) and financial support from HPSTAR. This work was supported by HLD-HZDR, member of the European Magnetic Field Laboratory (EMFL). We further acknowledge support under the European Union's Horizon 2020 research and innovation programme through the ISABEL project (No. 871106). A.V.S. acknowledges the financial support of RSF Grant No. 24-72-10109. This work was supported by the National Key Research and Development Program of China (Grant No. 2023YFA1608900, subproject 2023YFA1608903). The high-pressure experiments were supported by the state assignment of the Kurchatov Complex of Crystallography and Photonics (KKKiF). XRF analysis was performed using the equipment of the Shared Research Center of the Kurchatov Complex of Crystallography and Photonics. The authors acknowledge the European Synchrotron Radiation Facility (ESRF) for provision of synchrotron radiation facilities and Momentum Transfer for facilitating the measurements. Jakub Drnec was thanked for assistance and support in using beamline ID31. The measurement setup was developed with funding from the European Union's Horizon 2020 research and innovation program under the STREAMLINE project (grant agreement ID 870313). Measurements performed as part of the MatScatNet

project were supported by OSCARS through the European Commission's Horizon Europe Research and Innovation programme under grant agreement No. 101129751. We thank the staff members of the WMS (https://cstr.cn/31125.02.SHMFF.WM5) at the Steady High Magnetic Field Facility, CAS (https://cstr.cn/31125.02.SHMFF) for providing technical support and assistance in data collection and analysis. All authors thank the staff scientists of the SPring-8, Elettra, Xpress station (proposals Nos. 20215034 and 20220288) and the ESRF, station ID27 (proposal MA-5924), synchrotron radiation facilities for their help with X-ray diffraction measurements, especially Dr. Anna S. Pakhomova (ESRF), Dr. Saori Kawaguchi (SPring-8), Dr. Boby Joseph (Elettra), Prof. Katsuya Shimizu and Dr. Yuki Nakamoto (Osaka University).

Conflict of Interest

The authors declare no conflict of interest.

Author Contributions

D.V.S., I.A.T., and D.Z. contributed equally to this work. I.A.T., D.V.S., D.Z., M.G., A.V.S., O.A.S., A.G.I., A.S.P., F.G.-A., C.X., T.H., S.L., and K.P. performed the experiments. D.Z., M.G., and D.S. prepared the theoretical part of the paper. K.S.P. prepared the La–Sc alloys. A.G.I. analyzed the composition of La-Sc alloys. I.A.T. prepared diamond anvil cells for experiments. A.V.S., O.A.S., and V.M.P. performed the magnetotransport experiments in magnetic fields below 16 T and participated in the data processing and discussions. W.C. wrote scripts for critical current measurements. C.X. helped with Hall measurements in steady magnetic fields up to 33 T. T.H. and S.L. assisted in research in pulsed magnetic fields up to 68 T. A.S.P. and F.G.-A. performed X-ray diffraction studies. D.V.S., V.M.P., and V.V.S. wrote the manuscript. All the authors discussed the results and offered useful inputs.

Data Availability Statement

The data that support the findings of this study are available from the corresponding author upon reasonable request.

Keywords

high-pressure, SQUID hydride, superconductivity, superhydride

Received: February 28, 2025
Revised: April 19, 2025
Published online: August 1, 2025

[1] I. A. Troyan, D. V. Semenok, A. G. Ivanova, A. G. Kvashnin, D. Zhou, A. V. Sadakov, O. A. Sobolevsky, V. M. Pudalov, A. R. Oganov, *Phys. Usp.* **2022**, *65*, 748.
[2] I. Troyan, D. Semenok, A. Sadakov, I. Lyubutin, V. Pudalov, *JETP* **2024**, *139*, 74.
[3] A. P. Drozdov, M. I. Eremets, I. A. Troyan, V. Ksenofontov, S. I. Shylin, *Nature* **2015**, *525*, 73.
[4] I. A. Troyan, D. V. Semenok, A. G. Kvashnin, A. V. Sadakov, O. A. Sobolevskiy, V. M. Pudalov, A. G. Ivanova, V. B. Prakapenka, E. Greenberg, A. G. Gavriliuk, I. S. Lyubutin, V. V. Struzhkin, A. Bergara, I. Errea, R. Bianco, M. Calandra, F. Mauri, L. Monacelli, R. Akashi, A. R. Oganov, *Adv. Mater.* **2021**, *33*, 2006832.
[5] A. P. Drozdov, P. P. Kong, V. S. Minkov, S. P. Besedin, M. A. Kuzovnikov, S. Mozaffari, L. Balicas, F. F. Balakirev, D. E. Graf, V. B. Prakapenka, E. Greenberg, D. A. Knyazev, M. Tkacz, M. I. Eremets, *Nature* **2019**, *569*, 528.
[6] M. Somayazulu, M. Ahart, A. K. Mishra, Z. M. Geballe, M. Baldini, Y. Meng, V. V. Struzhkin, R. J. Hemley, *Phys. Rev. Lett.* **2019**, *122*, 027001.
[7] S. Chen, Y. Wang, F. Bai, X. Wu, X. Wu, A. Pakhomova, J. Guo, X. Huang, T. Cui, *J. Am. Chem. Soc.* **2024**.
[8] D. V. Semenok, B. L. Altshuler, E. A. Yuzbashyan, arXiv:2407.12922 **2024**.
[9] K. Trachenko, B. Monserrat, M. Hutcheon, C. J. Pickard, arXiv:2406.08129 **2024**.
[10] M. V. Sadovskii, *JETP Lett.* **2024**.
[11] P. W. Anderson, *J. Phys. Chem. Solids* **1959**, *11*, 26.
[12] L. P. Gor'kov in, *Superconductivity: Conventional and Unconventional Superconductors*, (Eds K. H. Bennemann, J. B. Ketterson), Springer, Berlin Heidelberg **2008**, 201–224.
[13] D. V. Semenok, I. A. Troyan, A. V. Sadakov, D. Zhou, M. Galasso, A. G. Kvashnin, A. G. Ivanova, I. A. Kruglov, A. A. Bykov, K. Y. Terent'ev, A. V. Cherepakhin, O. A. Sobolevskiy, K. S. Pervakov, A. Y. Seregin, T. Helm, T. Förster, A. D. Grockowiak, S. W. Tozer, Y. Nakamoto, K. Shimizu, V. M. Pudalov, I. S. Lyubutin, A. R. Oganov, *Adv. Mater.* **2022**, *34*, 2204038.
[14] D. V. Semenok, I. A. Troyan, A. G. Kvashnin, A. G. Ivanova, M. Hanfland, A. V. Sadakov, O. A. Sobolevskiy, K. S. Pervakov, A. G. Gavriliuk, I. S. Lyubutin, K. Glazyrin, N. Giordano, D. Karimov, A. Vasiliev, R. Akashi, V. M. Pudalov, A. R. Oganov, *Mater. Today* **2021**, *48*, 18.
[15] J. Bi, Y. Nakamoto, P. Zhang, Y. Wang, L. Ma, Y. Wang, B. Zou, K. Shimizu, H. Liu, M. Zhou, H. Wang, G. Liu, Y. Ma, *Mater. Today Phys.* **2022**, *28*, 100840.
[16] S. Chen, J. Guo, Y. Wang, X. Wu, W. Chen, X. Huang, T. Cui, *Phys. Rev. B* **2024**, *109*, 224510.
[17] K. Zhang, W. Chen, Y. Zhang, J. Guo, S. Chen, X. Huang, T. Cui, *Sci. China: Phys., Mech. Astron.* **2024**, *67*, 238211.
[18] S. Chen, Y. Qian, X. Huang, W. Chen, J. Guo, K. Zhang, J. Zhang, H. Yuan, T. Cui, *Natl. Sci. Rev.* **2023**, *11*, 107.
[19] Y. Song, J. Bi, Y. Nakamoto, K. Shimizu, H. Liu, B. Zou, G. Liu, H. Wang, Y. Ma, *Phys. Rev. Lett.* **2023**, *130*, 266001.
[20] L.-C. Chen, T. Luo, Z.-Y. Cao, P. Dalladay-Simpson, G. Huang, D. Peng, L.-L. Zhang, F. A. Gorelli, G.-H. Zhong, H.-Q. Lin, X.-J. Chen, *Nat. Commun.* **2024**, *15*, 1809.
[21] W. Chen, X. Huang, D. V. Semenok, S. Chen, D. Zhou, K. Zhang, A. R. Oganov, T. Cui, *Nat. Commun.* **2023**, *14*, 2660.
[22] J. Bi, Y. Nakamoto, P. Zhang, K. Shimizu, B. Zou, H. Liu, M. Zhou, G. Liu, H. Wang, Y. Ma, *Nat. Commun.* **2022**, *13*, 5952.
[23] X. Song, X. Hao, X. Wei, X.-L. He, H. Liu, L. Ma, G. Liu, H. Wang, J. Niu, S. Wang, Y. Qi, Z. Liu, W. Hu, B. Xu, L. Wang, G. Gao, Y. Tian, *J. Am. Chem. Soc.* **2024**.
[24] J. Guo, D. Semenok, G. Shutov, D. Zhou, S. Chen, Y. Wang, K. Zhang, X. Wu, S. Luther, T. Helm, X. Huang, T. Cui, *Natl. Sci. Rev.* **2024**, *11*, nwae149.
[25] S. Cross, J. Buhot, A. Brooks, W. Thomas, A. Kleppe, O. Lord, S. Friedemann, *Phys. Rev. B* **2024**, *109*, L020503.
[26] Q. Jiang, D. Duan, H. Song, Z. Zhang, Z. Huo, S. Jiang, T. Cui, Y. Yao, *Adv. Sci.* **2024**, *11*, 2405561.
[27] X. He, W. Zhao, Y. Xie, A. Hermann, R. J. Hemley, H. Liu, Y. Ma, *Proc. Natl. Acad. Sci. USA* **2024**, *121*, 2401840121.
[28] M. Kostrzewa, K. M. Szczęśniak, A. P. Durajski, R. Szczęśniak, *Sci. Rep.* **2020**, *10*, 1592.
[29] D. V. Semenok, I. A. Troyan, D. Zhou, W. Chen, H.-k. Mao, V. V. Struzhkin, *Innov. Mater.* **2025**, *3*, 100115.
[30] I. A. Troyan, D. V. Semenok, A. G. Ivanova, A. V. Sadakov, D. Zhou, A. G. Kvashnin, I. A. Kruglov, O. A. Sobolevskiy, M. V. Lyubutina, T. Helm, S. W. Tozer, M. Bykov, A. F. Goncharov, V. M. Pudalov, I. S. Lyubutin, *Adv. Sci.* **2023**, *10*, 2303622 .
[31] D. Semenok, *Ph.D. Thesis*, Skoltech (Moscow) **2022**.

[32] M. Shao, S. Chen, W. Chen, K. Zhang, X. Huang, T. Cui, *Inorg. Chem.* **2021**, *60*, 15330.
[33] M. A. Kuzovnikov, A. P. Drozdov, P. Kong, V. S. Minkov, S. P. Besedin, V. B. Prakapenka, E. Greenberg, D. A. Knyazev, M. I. Eremets, presented at 57th EHPRG Meeting on High Pressure Science and Technology, Crystal structures of novel lanthanum superhydrides, Prague, Czech Republic **2019**.
[34] D. Laniel, F. Trybel, B. Winkler, F. Knoop, T. Fedotenko, S. Khandarkhaeva, A. Aslandukova, T. Meier, S. Chariton, K. Glazyrin, V. Milman, V. Prakapenka, I. A. Abrikosov, L. Dubrovinsky, N. Dubrovinskaia, *Nat. Commun.* **2022**, *13*, 6987.
[35] Z. M. Geballe, H. Liu, A. K. Mishra, M. Ahart, M. Somayazulu, Y. Meng, M. Baldini, R. J. Hemley, *Angew. Chem., Int. Ed.* **2017**, *57*, 688.
[36] J. E. Hirsch, *J. Supercond.* **2023**, *36*, 1495.
[37] P. Hou, F. Belli, R. Bianco, I. Errea, *J. Appl. Phys.* **2021**, *130*, 175902.
[38] D. Zhou, D. Semenok, M. Galasso, F. G. Alabarse, D. Sannikov, I. A. Troyan, Y. Nakamoto, K. Shimizu, A. R. Oganov, *Adv. Energy Mater.* **2024**, *14*, 2400077.
[39] A. R. Oganov, C. W. Glass, *J. Chem. Phys.* **2006**, *124*, 244704.
[40] A. O. Lyakhov, A. R. Oganov, H. T. Stokes, Q. Zhu, *Comput. Phys. Commun.* **2013**, *184*, 1172.
[41] A. R. Oganov, R. O. Lyakhov, M. Valle, *Acc. Chem. Res.* **2011**, *44*, 227.
[42] Y. Wang, J. Lv, L. Zhu, Y. Ma, *Phys. Rev. B* **2010**, *82*, 094116.
[43] Y. Wang, J. Lv, L. Zhu, Y. Ma, *Comput. Phys. Commun.* **2012**, *183*, 2063.
[44] C. J. Pickard, R. J. Needs, *Phys. Rev. Lett.* **2006**, *97*, 045504.
[45] C. J. Pickard, R. J. Needs, *J. Phys.: Condens. Matter* **2011**, *23*, 053201.
[46] J. E. Hirsch, F. Marsiglio, *Phys. Rev. B* **2021**, *103*, 134505.
[47] A. V. Sadakov, V. A. Vlasenko, I. A. Troyan, O. A. Sobolevskiy, D. V. Semenok, D. Zhou, V. M. Pudalov, *J. Phys. Chem. Lett.* **2023**, *14*, 6666.
[48] A. V. Sadakov, V. A. Vlasenko, D. V. Semenok, D. Zhou, I. A. Troyan, A. S. Usoltsev, V. M. Pudalov, *Phys. Rev. B* **2024**, *109*, 224515.
[49] S. Mozaffari, D. Sun, V. S. Minkov, A. P. Drozdov, D. Knyazev, J. B. Betts, M. Einaga, K. Shimizu, M. I. Eremets, L. Balicas, F. F. Balakirev, *Nat. Commun.* **2019**, *10*, 2522.
[50] V. S. Minkov, V. Ksenofontov, S. L. Bud'ko, E. F. Talantsev, M. I. Eremets, *Nat. Phys.* **2023**, *19*, 1293.
[51] D. Sun, V. S. Minkov, S. Mozaffari, Y. Sun, Y. Ma, S. Chariton, V. B. Prakapenka, M. I. Eremets, L. Balicas, F. F. Balakirev, *Nat. Commun.* **2021**, *12*, 6863.
[52] E. F. Talantsev, V. Chistyakov, *Supercond. Sci. Technol.* **2024**, *37*, 095016.
[53] D. V. Semenok, W. Chen, X. Huang, D. Zhou, I. A. Kruglov, A. B. Mazitov, M. Galasso, C. Tantardini, X. Gonze, A. G. Kvashnin, A. R. Oganov, T. Cui, *Adv. Mater.* **2022**, *34*, 2200924.
[54] W. Chen, D. V. Semenok, A. G. Kvashnin, X. Huang, I. A. Kruglov, M. Galasso, H. Song, D. Duan, A. F. Goncharov, V. B. Prakapenka, A. R. Oganov, T. Cui, *Nat. Commun.* **2021**, *12*, 273.
[55] D. Semenok, J. Guo, D. Zhou, W. Chen, T. Helm, A. Kvashnin, A. Sadakov, O. Sobolevsky, V. Pudalov, V. Struzhkin, C. Xi, X. Huang, I. Troyan, arXiv:2307.11742v2 **2023**.
[56] N. D. Cottam, F. Wang, J. S. Austin, C. J. Tuck, R. Hague, M. Fromhold, W. Escoffier, M. Goiran, M. Pierre, O. Makarovsky, L. Turyanska, *Small* **2024**, *20*, 2311416.
[57] A. Cucciari, D. Naddeo, S. Di Cataldo, L. Boeri, *Phys. Rev. B* **2024**, *110*, L140502.
[58] E. F. Talantsev, *Matter Radiat. Extremes* **2022**, *7*, 058403.
[59] Y. Zhou, J. Guo, S. Cai, H. Sun, C. Li, J. Zhao, P. Wang, J. Han, X. Chen, Y. Chen, Q. Wu, Y. Ding, T. Xiang, H.-K. Mao, L. Sun, *Matter Radiat. Extrem.* **2025**, 10.
[60] P. Allen, R. Dynes, *Techn. Rep.* **1974**, *7*, TCM/4/1974.
[61] C. Pellegrini, A. Sanna, *Nat. Rev. Phys.* **2024**, *6*, 509.
[62] A. B. Migdal, *Sov. Phys. JETP* **1958**, *7*, 996.
[63] G. M. Eliashberg, *Sov. Phys. JETP* **1960**, *11*, 696.
[64] A. V. Sadakov, V. A. Vlasenko, I. A. Troyan, O. A. Sobolevskiy, D. V. Semenok, D. Zhou, V. M. Pudalov, *J. Phys. Chem. Lett.* **2023**, *14*, 6666.
[65] P. J. W. Moll, V. B. Geshkenbein, *Nat. Phys.* **2023**, *19*, 1379.
[66] D. V. Semenok, A. V. Sadakov, D. Zhou, O. A. Sobolevskiy, S. Luther, T. Helm, V. M. Pudalov, I. A. Troyan, V. V. Struzhkin, *Mater. Today Phys.* **2024**, *49*, 101595.
[67] Y. A. Timofeev, V. V. Struzhkin, R. J. Hemley, H.-K. Mao, E. A. Gregoryanz, *Rev. Sci. Instrum.* **2002**, *73*, 371.
[68] Y. L. Wu, X. H. Yu, J. Z. L. Hasaien, F. Hong, P. F. Shan, Z. Y. Tian, Y. N. Zhai, J. P. Hu, J. G. Cheng, J. Zhao, *Nat. Commun.* **2024**, *15*, 9683.
[69] V. Struzhkin, B. Li, C. Ji, X.-J. Chen, V. Prakapenka, E. Greenberg, I. Troyan, A. Gavriliuk, H.-K. Mao, *Matter Radiat. Extremes* **2020**, *5*, 028201.